Nature geosciences
October 2022, Volume 15, Pages 919-924
https://doi.org/10.1038/s41561-022-01048-4
https://archimer.ifremer.fr/doc/00799/91125/

High rates of organic carbon burial in submarine deltas maintained on geological timescales

Hage Sophie [1, 2, *], Romans Brian [3], Peploe Thomas [1], Poyatos-Moré Miquel [4], Haeri Ardakani Omid [1, 5], Bell Daniel [1], Englert Rebecca [1], Kaempfe-Droguett Sebastian [3], Nesbit Paul [1], Sherstan Georgia [1], Synnott Dane [1], Hubbard Stephen [1]

[1] Department of Geoscience, University of Calgary, Calgary, Alberta, Canada
[2] Geo-Ocean, Univ. Brest, CNRS, Ifremer, Finistère, France
[3] Department of Geosciences, Virginia Tech, Blacksburg, VA, USA
[4] Departament de Geologia, Universitat Autònoma de Barcelona, Cerdanyola del Vallès, Spain
[5] Natural Resources Canada, Geological Survey of Canada, Calgary, Alberta, Canada

* Corresponding author : Sophie Hage, email address : sophie.hage@univ-brest.fr

Abstract :

Burial of terrestrial organic carbon in marine sediments can draw down atmospheric CO2 levels on Earth over geologic timescales (≥105 yr). The largest sinks of organic carbon burial in present-day oceans lie in deltas, which are composed of three-dimensional sigmoidal sedimentary packages called clinothems, dipping from land to sea. Analysis of modern delta clinothems, however, provides only a snapshot of the temporal and spatial characteristics of these complex systems, making long-term organic carbon burial efficiency difficult to constrain. Here we determine the stratigraphy of an exhumed delta clinothem preserved in Upper Cretaceous (~75 million years ago) deposits in the Magallanes Basin, Chile, using field measurements and aerial photos, which was then combined with measurement of total organic carbon to create a comprehensive organic carbon budget. We show that the clinothem buried 93 ± 19 Mt terrestrial-rich organic carbon over a duration of 0.1–0.9 Myr. When normalized to the clinothem surface area, this represents an annual burial of 2.3–15.7 t km−2 yr−1 organic carbon, which is on the same order of magnitude as modern-day burial rates in clinothems such as the Amazon delta. This study demonstrates that deltas have been and will probably be substantial terrestrial organic carbon sinks over geologic timescales, a long-standing idea that had yet to be quantified.

Keywords : Carbon cycle, Geochemistry, Sedimentology

Atmospheric CO_2 can be consumed into terrestrial organic carbon (OC) by plants and algae through photosynthesis on land. A small fraction of this organic carbon is transported by rivers to the ocean as particulate organic carbon at a global present-day annual rate between 170 and 200 Mt OC yr^{-1} (refs. 1, 2). The burial rate of terrestrial OC into marine sediments is estimated at 58 ± 17 Mt OC yr^{-1} (ref. 3), representing the second largest sink of atmospheric CO_2 after silicate weathering[4]. Thus, it regulates climate over geologic timescales (i.e., ≥ 10^5 years[5,6,7]). Deltas and associated shelfal deposits hold between 70 and 90 % of the global OC burial budget in marine sediments[8,9,3,10]. Among major river deltas, the Amazon represents the largest supplier of terrestrial OC to the global ocean (31 x 10^{12} to 54.8 x 10^{12} g OC yr^{-1})[2,11] whereas the annual OC burial flux of the Ganges-Brahmaputra subaqueous delta contains 10 to 20% of the total terrestrial OC annual burial flux in marine sediments globally[5]. Human activities are currently modifying the dynamics of deltas including their ability to migrate seaward (i.e., prograde[12]), which can lead to a decrease in present-day carbon storage fluxes (e.g., Mississippi delta[10]). However, the carbon storage potential of deltas is, for now, poorly constrained over geologic timescales.

Progradation of large river deltas produces sigmoidal depositional surfaces dipping from shallow to deeper waters, called clinoforms[13], which have been identified in both Holocene and ancient deltaic successions[14]. Clinoforms are usually divided into three segments: *topsets* form the shallower-water segment and have gentle slopes that pass basinward into steeper *foresets*, which terminate onto gently dipping *bottomsets* in deeper waters[15]. Clinoforms bound packages of strata termed clinothems, which can develop over a range of spatial and temporal scales (10^2 to 10^8 years[14,15]). Topset, foreset, and bottomset strata are each defined by specific sedimentary characteristics, and accumulation rates ranging from < 1 mm yr^{-1} in topsets and bottomsets, to up to 100 mm yr^{-1} in foresets[14, 16,17](suppl. Table S1). Despite the global significance of deltaic clinothems such as those forming the Amazon and Ganges-Brahmaputra deltas, their OC storage potential has not been investigated in three dimensions, nor over geologic timescales. Clinothems dominate deltaic-to-continental margin successions and their

architectures evolve over time influenced by sediment supply, relative sea-level, tectonic activity, and climate variability[14,18,19,20]. However, these long-term influences are not captured in surficial sediment of present-day delta clinothems, which only include a snapshot of their history, making their long-term terrestrial OC burial efficiency difficult to constrain. An effective approach to test whether OC can be stored in river deltas over geologic timescales is through the study of exhumed ancient deltaic successions. Long-term OC content has been reported from ancient, outcropping delta clinothems to constrain their petroleum source-rock characteristics[21,22]. However no study has considered how the global carbon cycle is impacted through the long-term ($\geq 10^5$ yr) evolution of a deltaic system using exhumed deposits.

Here we present a detailed quantification of OC in an ancient, exhumed delta. This study is performed using a 525 m-thick stratigraphic section, sampled at sub-5 m intervals. The section exposes deposits of an Upper Cretaceous delta clinothem succession that is oriented in a proximal-distal transect extending 3000 m in length, 100's m thick and spanning 10^5 to 10^6 years, from the Magallanes sedimentary basin in southern Chile. Using this data, we question: How much OC is buried in an ancient delta? How does OC abundance and composition vary within deltaic stratigraphy? We finally discuss the implications of our findings for the global carbon cycle by comparing past and present terrestrial OC fluxes buried in deltaic marine sediments.

Unique exposure of delta clinothems in the Magallanes Basin

The sigmoidal profile of ancient clinothems can be recognized in topographic profiles at a variety of scales, from smaller shelf deltas (10's m relief) that build into shallow water to larger deltas (100's m relief) that build onto continental margins[23]. The largest ancient clinothems are most frequently observed in seismic reflection datasets[24,25,19], whereas outcrops most commonly expose partial and/or smaller delta clinothems, due to scale limitations and their propensity to occur in shallow-water

foreland basin successions[15]. Here we use a unique outcrop exposure of large-scale (100s of m thick) clinothems from the Campanian to Maastrichtian (80-72 Ma) Tres Pasos and Dorotea formations of the Magallanes Basin at the southern end of the Andean Cordillera, Chile[26,27] (Fig. 1, Extended Data Fig.1). The Magallanes foreland basin is filled with >4 km of deep-to-shallow-water sediments deposited during a prolonged period of subsidence coupled with high sediment supply, which resulted from the uplift and denudation of an active fold-thrust belt[28,29].

In this study we focus on a series of deltaic clinothems that record the terminal infill of the marine depocenter (Oveja and Puma clinothems[27]; Fig. 1c). The studied strata record deltaic deposition into 100s of m of water depth, with consequent 100s of m-thick and a kms-long clinothems that record 10^4 to 10^5 years of deposition[27]. We use a 525 m-thick stratigraphic section located on Cerro Cazador (Figs. 1b and 3a), which intersects three clinothems within the Oveja interval from bottom to top (Fig. 1e). Sedimentary characteristics such as grain size, bed thickness, and depositional structures were recorded at 10 cm resolution. Clinothem 1 comprises 55 m of mudstone-dominated bottomset deposits, clinothem 2 comprises 235 m of poorly to moderately sorted, siltstone to very fine sandstone foreset deposits, and clinothem 3 comprises 80 m of sandstone-dominated topset deposits (Figs. 1d). Topset, foreset, and bottomset deposits from these three clinothems were considered collectively to form a composite clinothem set record (Figs. 2a and 3a), from which a comprehensive OC burial budget is estimated. Each clinothem is ~3 km-long (i.e., along dip) and estimated between 6 km (i.e., two times the clinothem length[30]) and 20 km-wide (i.e., across-shelf corresponding to the width extent of the Magallanes Basin[26]; see methods, Extended Data Figs 2 and 3). Thickness and length dimensions were measured from a photogrammetry model acquired with an uncrewed aerial vehicle (UAV) and processed in Pix4D software using high-precision ground control points measured in the field (Extended Data Fig. 2; ref. 31). The duration of each clinothem is estimated to range between 0.1 and 0.9 Myr (Table 1), based on sediment accumulation rate measurements from analogous clinothems over a range

of timescales (10^1 to 10^6 yrs[16,17,32], Extended Data Table 1). These durations are further and independently supported by ages obtained using U-Pb geochronology that gave a duration value of 0.5 ± 1.7 Myr for the studied clinothems[33].

Mass and rate of organic carbon burial in a delta clinothem

A total of 99 samples were collected at sub-5 m intervals through the 525 m-thick section (Figs. 1e and 3a). All samples were ground into powder and measured for total organic carbon (TOC) content by programme pyrolysis and an elemental analyser (see Methods). The composite clinothem set has an average TOC of 0.72 ± 0.24 %, with a general upwards decreasing trend (Figs. 2b and 3b, Table 1). TOC (in wt %) varies as follows: 0.81 ± 0.11% (n = 11 samples) in the bottomset, 0.75 ± 0.32% (n = 31 samples) in the foreset, and 0.48 ± 0.16% (n = 47 samples) in the topset segment of the composite clinothem (Fig. 2b). The lower TOC in the topset is consistent with present-day deltas where topset regions are commonly areas of sediment bypass, resulting in variable but generally minimal preservation[19,34] Using a quartz sediment density of 2650 kgm^{-3}, an average porosity of 5% in the mudstone-dominated and 20% in the sandstone-dominated segments[35], and the measured dip cross-sectional area of a typical clinothem in Cerro Cazador (see Methods), we show that over 0.1 to 0.9 Myr, one clinothem includes 93 ± 19 Mt OC (Table 1). Approximately 68% of the OC is buried in foreset deposits while the topset and bottomset deposits include ~15 and ~17%, respectively (Extended Data Table 2). Based on annual sediment accumulation rates in analogous subaqueous deltaic settings[16,17,32], we calculate an annual burial organic carbon flux ranging from 0.13 to 0.87 kt OC yr^{-1} (Table 1). When normalized to the surface area of the composite clinothem (57 ± 38 km^2; Table 1), the annual OC burial yield of the Upper Cretaceous delta clinothem ranges from 2.3 ± 0.5 to 15.2 ± 3.5 t OC km^{-2} yr^{-1}. These OC yields calculated for our ancient delta are of similar magnitude to the estimated area-normalized burial yields of present-day global continental shelves (~6 t OC km^{-2} yr^{-1}; refs. 36, 37, Fig. 2c) and in the lower limits of the yield of present-day deep-sea fans (e.g., Congo[38] , Rhone[39] and Amazon[40] deep-sea

fans ; Fig. 2c) and fjords[38,41,42]. This demonstrates that delta clinothems, particularly their foresets segments (Extended Data Table 2), are globally important sinks of OC burial over geologic timescales.

Variation of organic carbon abundance and composition in context of deltaic stratigraphic architecture

The abundance of OC decreases up section, i.e., from bottomset to topset segments in the composite clinothem (Fig. 3b). Overall, the section comprises OC that is mostly terrigenous in origin, supported by multiple independently measured proxies (Fig. 3, Extended Data Figs. 4, 5 and 6). First, OC stable isotope ratios ($\delta^{13}C_{org}$) were measured using an isotope ratio mass spectrometer (IRMS) on decarbonated samples, with a mean $\delta^{13}C_{org}$ value of -25.56 ± 0.35‰ (Fig. 3c). Typically, the $\delta^{13}C_{org}$ signature of terrigenous C3 plants is between -24 and -30 ‰[43,44]. The topset deposits have a slightly more depleted $\delta^{13}C_{org}$ composition (-25.75 ± 0.3 ‰) compared to the bottomset deposits (-25.35 ± 0.2‰), which could indicate the presence of mixing with marine OC in the bottomsets, typically ranging between -18 and -24‰[43]. Second, programmed pyrolysis-derived hydrogen index[45,46,47] (HI, Fig. 3d, methods) is low for all samples (< 50), which, at the thermal maturity of the analyzed samples is likely indicative of a terrigenous origin[38,43]. Third, organic petrographic observations (Fig. 3e) show the abundant presence of terrigenous macerals (e.g., vitrinite and inertinite) that are derived from higher land plants[49,50]. Marine macerals (e.g., alginate and bituminite) are present, particularly in bottomset samples, and confirm the presence of marine organic matter, typically bacteria and algae of planktonic origin[51]. Finally, the *n*-alkane biomarkers extracted from 12 samples (methods, Extended Data Fig. 6b) all present a terrigenous to aquatic ratio (TAR[48]) > 1, further supporting the dominance of terrigenous OC in the studied clinothem. Evidence for an upward TOC-decrease and terrestrial OC-increase trends are consistent with the overall progradational trend of the deltaic deposits from land to sea[27]. Smaller-scale TOC and $\delta^{13}C_{org}$ oscillations compared to this overall trend are observed in the stratigraphic section (Fig. 3), which belong to higher-frequency variability that might be related to relative sea-level changes, climate, and/or tectonics[18].

Programmed pyrolysis data and vitrinite reflectance measurements reveal that organic matter in our stratigraphic section is relatively immature, ranging from immature to early catagenesis[46] (see methods; Extended Data Fig. 6c). This implies a low burial depth and/or temperature, a low degree of recycling, and a short sediment transit time. Efficient transport and rapid sequestration of terrestrial OC along the Adriatic shelf during the Little Ice Age, for example, has been suggested to result from a direct connection between river sources and clinothems[19]. Such transport processes were likely prevalent in the Upper Cretaceous delta documented in this study [27]. It is worth noting that our dataset emphasizes the vertical variability of the OC abundance and type but does not directly capture the potential lateral variability that has been observed in modern systems[19]. Nonetheless, the long time span covered by our section combined with the relatively narrow basin setting[26] likely encompasses the range of 3D variability[52].

Implications for the global carbon cycle

Carbon is exchanged between the atmosphere, biosphere, and the solid Earth through multiple mechanisms that occurred over a range of timescales[7]. For example, photosynthesis by plants removes CO_2 from the atmosphere over short timescales ($< 10^4$ yr), whereas oxidative weathering of petrogenic OC from fossil ($\geq 10^5$ to 10^6 yr old) rocks returns CO_2 to the atmosphere[53,7]. As these mechanisms take place on different timescales, it is difficult to constrain their effects on the global carbon cycle based solely on Holocene sediments, where only short-term processes can be measured with certainty. In this study, although short-term mechanisms could not be directly determined, our calculations indicate that the rates of OC buried in Upper Cretaceous (75 Myr old) delta deposits (2.3 to 15.7 t OC km^{-2} yr^{-1}) are within the same order of magnitude as OC burial rates of Holocene delta deposits (2 to 140 t OC km^{-2} yr^{-1}; refs. 37 - 42). This further demonstrates that high organic carbon burial efficiency on deltas can be maintained over geologic timescales. We thus highlight the importance of present-day delta clinothems formed by major rivers (e.g. Ganges-Brahmaputra, Amazon, Rhone, Mississippi) and small rivers when

combined[54], as natural CO_2 sinks over a range of timescales. Protecting the world's deltas is thus crucial not only for present-day carbon storage[10,12] but also for maintaining their natural ability to sequester organic carbon over thousands to millions of years.

Acknowledgements

We thank Don Francisco, Lucy and Alejandro Cárdenas at Rincon Negro Ranch as well as Jose Luis and Manuel at San Luis Ranch for allowing us to access their lands. We also thank the Alvarez-Roehrs family for our stay at Hotel Tres Pasos and helpful advice. We are grateful to Steve Taylor (Isotope Science Lab) and Kimberley Nightingale (Petroleum Reservoir Group) at the University of Calgary for their precious help in labs. We thank Associate Editor James Super, Mike Shields, Claudio Pellegrini and two anonymous reviewers for providing feedback on this work.

Funding: Support for this research was provided by a Natural Sciences and Engineering Research Council of Canada Discovery Grant (RGPIN-2018-04223) held by S. Hubbard, as well as the Chile Slope Systems Joint Industry Project. Funding for organic petrography is provided by Natural Resources Canada (NRCan) provided by Geoscience for New Energy Supply (GNES). SH has received funding from the European Union's Horizon 2020 research and innovation programme under the Marie Sklodowska-Curie grant agreement No 899546.

Author contributions: S.H., B.W.R., S.M.H., M.P-M. designed the study. S.H., T.G.E.P., B.W.R., S.M.H., M.P-M, D.B., R.G.E., S.A.K., P.R.N collected the field data. S.H., O.H.A., G.S., D.P.S. collected the organic geochemistry and petrology data. S.H., B.W.R., T.G.E.P., S.M.H., M.P-M., O.H.A., D.P.S. analysed the data. P.R.N., T.G.E.P., R.G.E processed the UAV model. S.H. produced the figures. S.H., B.W.R., S.M.H. wrote the manuscript, with contributions from all authors.

Competing interests: The authors declare that they have no competing interests.

Tables

a. Organic Carbon (OC) mass = TOC/100 * D * W * (1-φ/100) * ρ					
TOC: total organic carbon (wt %)	D: dip cross sectional area (km^2)	W: clinothem width (km)	φ: porosity (%)	ρ: density ($kg\ m^{-3}$)	OC mass (Mt OC)
0.7 *± 0.24*	0.47	**13** *± 7*	**18** *± 8*	2650	**93** *± 19*

b. Organic Carbon (OC) annual flux = TOC/100 * A * SR * (1-φ/100) * ρ				
	A: Surface area (km^2)	SR: Sedimentation rate ($mm\ yr^{-1}$)	OC annual flux (kt OC yr-1)	OC annual yield (i.e. flux per surface area) ($ton\ OC\ km^{-2}\ yr^{-1}$)
Minimum estimate (i.e.. duration of 0.9 Myr)	**57** *± 38*	0.15	**0.13** *± 0.03*	**2.3** *± 0.5*
Maximum estimate (i.e.. duration of 0.1 Myr)		1	**0.89** *± 0.2*	**15.7** *± 3.5*

Table 1|a. Mass of organic carbon (OC) buried in the studied clinothem**.** Mean values are in bold, standard deviations are in italic. Dip cross sectional area and density values are measured, fixed values, thus there is no associated error range. **b.** Annual flux of OC calculated based on two scenarios for sedimentation rates (SR): 1) SR estimated based on ancient delta clinothems and 2) SR estimated based on Holocene delta clinothems. Durations are estimated based on the SR and the average thickness of the clinothem (130 m). OC yield is calculated by dividing the annual OC flux by the clinothem surface area. TOC corresponds to the weighted average based on dip cross sectional area of the clinothem segments (topset, foreset, bottomset). See methods for more detail on SR and clinothem duration. Mean values are in bold, standard deviations are in italic. Sedimentation rates estimates are presented in Extended Data Table 1.

Figures

Figure 1| Geographic and geologic context for this study. a. Location of the Magallanes Basin in southern Patagonia, Chile. **b.** Satellite view of the study area (Google Earth 7.3.4.8642, 2015). Deposits of the Tres Pasos and Dorotea Formations crop out in a north-south-oriented belt on the eastern flank of the Andes. The white triangle shows the location of Cerro Cazador. **c.** Interpreted regional cross-section of the clinoforms of the Tres Pasos and Dorotea formations at Cerro Cazador (modified from ref. 27). **d.** Schematic block diagram displaying the interpreted deltaic deposits in the studied strata (see Extended Data Fig.2 for details) **e.** Photograph of the central part of Cerro Cazador including the location of our studied section (in red). The geologic log of the section is displayed in Fig. 3a.

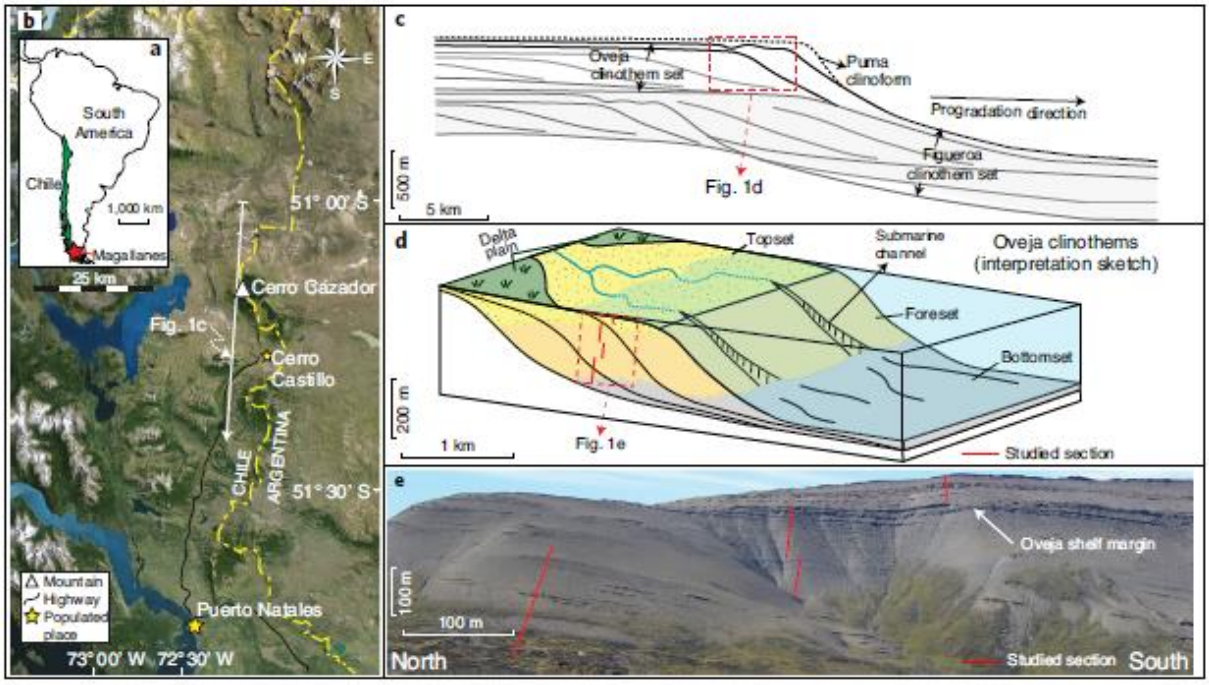

Figure 2| Organic carbon content and composition in the studied delta clinothem. a. Schematic representation of the studied clinothem. **b.** Mean total organic carbon (TOC) content (colored bars) for the topset, foreset and bottomset clinothem segments. Dots represent the measured TOC on each sample. Vertical bar represent the standard deviation for each segment. n = number of samples used to calculate the mean TOC for each segment. **c**: Comparison between area-normalized organic carbon burial yields for global continental shelves[37] , fjords[36,42], and deep sea Congo fan[38] (Baudin et al., 2020), Rhone fan[39], Amazon fan[40] and this study (based on the approach described in Table 1 and Extended Data Table 1).

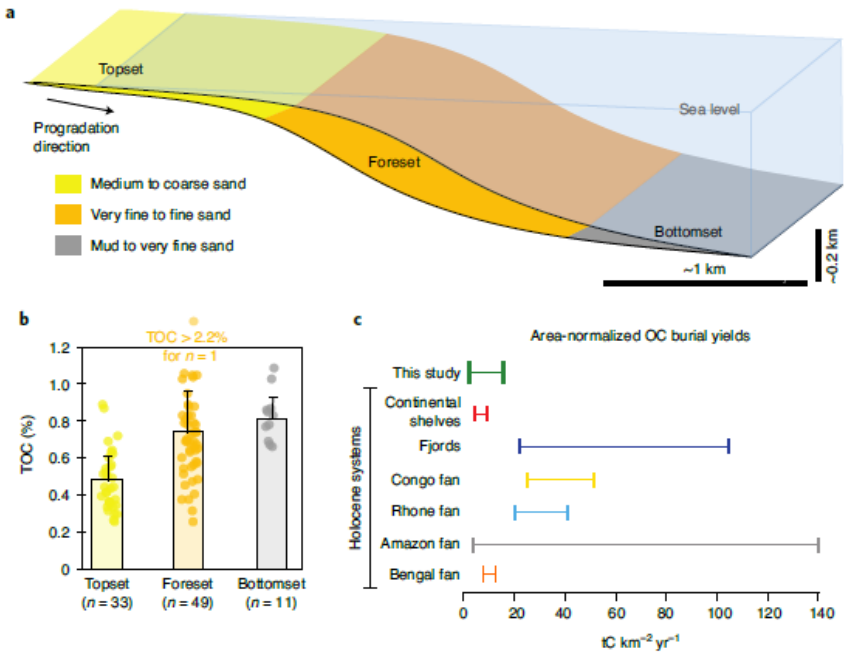

Figure 3| Stratigraphic section and bulk organic geochemistry. a: Simplified measured section at Cerro Cazador (Fig. 1e). Black line: 10 m-moving average of the grain size observed in the field. Grey, orange, and yellow colors highlight the dominance of mud and silt (< 62.5 µm), very fine sand (between 62.5 and 125 µm), and sand particles greater than 125 µm. Red lines are the moving averages over 5 measurements. **b.** Total organic carbon (TOC) distribution (wt %). **c.** Organic carbon stable isotope ratio ($\delta^{13}C_{org}$ ‰). **d.** Hydrogen Index (mg HC / g TOC). **e.** Photomicrographs of observed macerals in reflected white light (B and C) and UV light (D). Alg = Alginite, Bit = Bituminite, Ine = Inertite, Lip = liptinite, Vit = Vitrinite. Images were taken from samples shown in Fig. 2. Vitrinite and inertinite are interpreted to be terrigenous-derived whereas bituminite and liptinite are of marine origin.

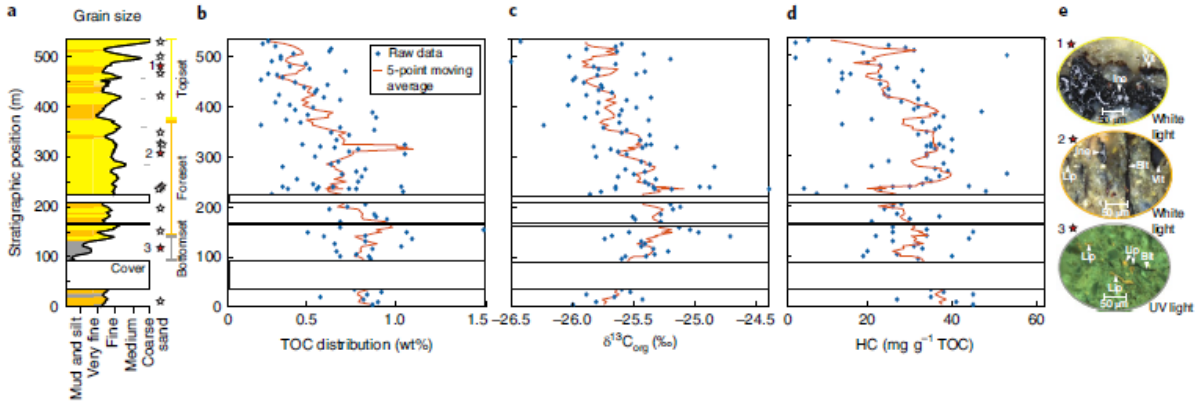

References

1. Ludwig, W., Probst, JL, Kempe, S. Predicting the oceanic input of organic carbon by continental erosion. *Glo. Biogeochem. Cycles* **10**, 23-41 (1996).
2. Schlünz, B. & Schneider, R. R. Transport of terrestrial organic carbon to the oceans by rivers: Re-estimating flux and burial rates. *Int. J. Earth Sci*. **88**, 599–606 (2000).
3. Burdige, DJ. Preservation of organic matter in marine sediments: controls, mechanisms, and an imbalance in sediment organic carbon budgets? *Chem. Rev.* **107**, 467-485 (2007).

4. Gaillardet, J., Dupre, B, Allegre CJ. Geochemistry of large river-suspended sediments: silicate weathering recycling tracer. *Geochim. Cosmochim. Acta* **63**, 4037–51 (2009).
5. Galy, V., France-Lanord, C., Beyssac, O., Faure, P., Kudrass, H., Palhol, F. Efficient organic carbon burial in the Bengal fan sustained by the Himalayan erosional system. *Nature* **450**, 407–410 (2007).
6. Blair, N.E. and Aller, R.C. The fate of terrestrial organic carbon in the marine environment. *Ann. Rev. Mar. Sci.* **4**, 401-423 (2012).
7. Hilton, R.G., and West, J.A. Mountains, erosion and the carbon cycle. *Nature Rev. Earth & Env.* **1**, 284-299 (2020).
8. Berner, RA. Burial of organic carbon and pyrite in the modern ocean – its geochemical and environmental significance. *Am. J. Sci.* 282, 451-473 (1982).
9. Hedges, J. I. & Keil, R. G. Sedimentary organic matter preservation: An assessment and speculative synthesis. *Mar. Chem.* **49**, 81–115 (1995).
10. Shields, M. R., Bianchi, T.S., Mohrig, D., Htchings, J.A., Kenney, W.F., Kolker, A.S., Curtis, J.H. Carbon storage in the Mississippi River delta enhanced by environmental engineering. *Nat. Geoscience* **10**, 846-851 (2017).
11. Richey, J.E., Brocl., J.T., Naiman, R.J., Wissmar, R.C., Stallard, R.F. Organic carbon: oxidation and transport in the Amazon River. *Science* **207**, 1348-1351 (1980).
12. Syvitski, J.P.M., Kettner, A.J., Overeem, I., Hutton, E.W.H., Hannon, M.T., Brakenridge, G.R., Day, J., Vorosmarty, C., Saito, Y., Giosan, L., Nicholls, R.J., Sinking deltas due to human activities. *Nat. Geoscience* **2**, 681-686 (2007).
13. Rich, J.L. Three critical environments of deposition and criteria for recognition of rocks deposited in each of them. *GSA Bulletin* **62**, 1-20 (1951).

14. Patruno, S. Hampson, G.J., Jackson, C.A. Quantitative characterisation of deltaic and subaqueous clinoforms. *Earth Sci. Rev.* **142**, 79-119 (2015).
15. Steel, R.J., Olsen, T., Clinoforms, clinoform trajectory and deepwater sands. In: Armentrout, J.M., Rosen, N.C. (Eds.), Sequence Stratigraphic Models for Exploration and Production: Evolving Methodology, Emerging Models and Application Histories. *GCS-SEPM Special Publication*, 367–381 (2002).
16. Kuehl, S.A., Nittrouer, C.A., DeMaster, D.J. Nature of sediment accumulation on the Amazon continental shelf. *Cont. Shelf Res.* **6**, 209–225 (1986)
17. Kuehl, S.A., Levy, B.M., Moore, W.S., Allison, M.A. Subaqueous delta of the Ganges-Brahmaputra river system. *Mar. Geol.* **144**, 81–96 (1997).
18. Steel, R. J., Carvajal, C., Petter, A. L., Uroza, C., Hampson, G. J., Burgess, P. M., & Dalrymple, R. W. Shelf and shelf-margin growth in scenarios of rising and falling sea level. *Recent advances in models of siliciclastic shallow-marine stratigraphy* **90**, 47-71 (2008).
19. Pellegrini, C., Tesi, T., Schieber, J., Bohacs, K.M., Rovere, M., Asioli, A., Nogarotto, A., and Trincardi, F. Fate of terrigenous organic carbon in muddy clinothems on continental shelves revealed by stratal geometries: Insight from the Adriatic sedimentary archive. *Global & Planetary Change* **203** (2021)
20. Trincardi, F., Amorosi, A., Bosman, A., Correggiari, A., Madricardo, F., & Pellegrini, C. (2020). Ephemeral rollover points and clinothem evolution in the modern Po Delta based on repeated bathymetric surveys. Basin Research, 32(Clinoforms and Clinothems: Fundamental Elements of Basin Infill), 402-418.)
21. Johnson Ibach, L.E. Relationship Between Sedimentation Rate and Total Organic Carbon Content in Ancient Marine Sediments. *AAPG Bulletin* **66** (2): 170–188. (1982)

22. Sageman, B.B., Gardner, M.H., Armentrout, J.M., Murphy, A.E. Stratigraphic hierarchy of organic carbon-rich siltstones in deep-water facies, Brushy Canyon Formation (Guadalupian), Delaware Basin, West Texas. *Geology* **26 (5)**, 451-454 (1988).
23. Swenson, J.B., Paola, C., Pratson, L., Voller, V.R., Murray, A.B. Fluvial and marine controls on combined subaerial and subaqueous delta progradation: morphodynamic modeling of compound-clinoform development. *J. Sed. Research: Earth Surface* **110** (F2) (2005).
24. Houseknecht, D.W., Bird, K.J., Schenk, C.J. Seismic analysis of clinoform depositional sequences and shelf-margin trajectories in Lower Cretaceous (Albian) strata, Alaska North Slope. *Basin Res.* **21 (5)**, 644–654 (2009).
25. Loseth, H., Dowdesdell, J.A., Batchelor, C.L., Ottesen, D. 3D sedimentary architecture showing the inception of an Ice Age. *Nature Comm.* **11**: 2975 (2020)
26. Hubbard, S. M., Fildani, A., Romans, B. W., Covault, J. A., and McHargue, T. R. (2010). High-relief slope clinoform development: insights from outcrop, Magallanes Basin, Chile*. J. Sed. Res*. **80**, 357–375 (2010).
27. Bauer, D.B., Hubbard, S.M., Covault, J.A., Romans, B.W. Inherited depositional topography control on shelf-margin oversteepening, readjustment, and coarse-grained sediment delivery to deep water, Magallanes Basin, Chile. *Front. Earth. Sci.* **7**: 358 (2020).
28. Romans, B. W., Fildani, A., Graham, S. A., Hubbard, S. M., and Covault, J. A. Importance of predecessor basin history on the sedimentary fill of a retroarc foreland basin: provenance analysis of the Cretaceous Magallanes Basin, Chile (50-52). *Basin Res.* **22**, 640–658. (2010).
29. Fosdick, J. C., Romans, B. W., Fildani, A., Bernhardt, A., Calderon, M., and Graham, S. A. Kinematic evolution of the Patagonian retroarc fold-and thrust belt and Magallanes foreland basin, Chile and Argentina, 51°30'S. *Geol. Soc. Am. Bull.* **123**, 1679–1698 (2011).

30. Graham, G.H., Jackson, M.D., and Hampson, G.J., Three-dimensional modeling of clinoforms in shallow-marine reservoirs: Part 1. Concepts and applications. *AAPG Bulletin* **99**(6), 1013-1047 (2015).
31. Nesbit, P.R., Hubbard, S.M., Daniels, B.G., Bell, D., Englert, R.G. and Hugenholtz, C.H., 2021. Digital re-evaluation of down-dip channel-fill architecture in deep-water slope deposits: Multi-scale perspectives from UAV-SfM. Depos. Rec. **7**, 480-499.
32. Palinkas, C.M., & Nittrouer, C.A. Clinoform sedimentation along the Apennine shelf, Adriatic Sea. *Mar. Geol.* **234**, 245-260 (2006).
33. Daniels, B. G., Auchter, N. C., Hubbard, S. M., Romans, B. W., Matthews, W. A., and Stright, L. Timing of deep-water slope evolution constrained by large-n detrital zircon and volcanic ash geochronology, Cretaceous Magallanes Basin, Chile. Bull. Geol. Soc. Am. **130**, 438–454 (2018).
34. Goni, M.A., Monacci, N., Gisewhite, R., Crockett, J., Nittrouer, C., Ogston, A., Alin, S.R., Aalto, R. Terrigenous organic matter in sediments from the Fly River delta-clinoform system (Papua New Guinea). Journal of Geophysical Research, **113**, F01S10 (2008)
35. Howell, J.A., Skorstad, A., MacDonald, A. Fordham, A., Flint, S. Fjellvoll, B. and Manzocchi, T. Sedimentological parameterization of shallow-marine reservoirs. *Petro. Geosci.* **14**, 17-34 (2008).
36. Smith, R. W., Bianchi, T. S., Allison, M., Savage, C., & Galy, V. High rates of organic carbon burial in fjord sediments globally. Nature Geoscience **8** (2015).
37. Yool, A. and Fasham, M.J.R. An examination of the “continental shelf pump” in an open ocean general circulation model. Global Biogeochemical cycles **15**, 831-844 (2001)
38. Baudin, F., Rabouille, C., & Dennielou, B. (2020). Routing of terrestrial organic matter from the Congo River to the ultimate sink in the abyss: a mass balance approach (André Dumont medallist lecture 2017). *Geologica Belgica* **23**(1-2).

39. Durrieu de Madron, X., Abassi, A., Heussner, S., Monaco, A., Aloisi, JC, Radakovitch, O., Giresse, P., Buscail, R., Kerherve, P., Particulate matter and organic carbon budgets for the Gulf of Lions (NW Mediterranean). *Oceanologica Acta* **23** (6), (2000).

40. Schlünz B, Schneider RR, Müller PJ, Showers WJ, Wefer G. Terrestrial organic carbon accumulation on the Amazon Deep Sea Fan during the last glacial sea-level low stand. *Chem Geol*. **159**, 263–281 (1999).

41. Cui, X., Bianchi, T. S., Savage, C., Smith, R.W. Organic carbon burial in fjords: terrestrial versus marine inputs. *Earth and Planetary Science Letters* **451**, 41-50. (2016)

42. Smeaton, C., & Austin, W. E. N. (2019). Where's the Carbon: Exploring the Spatial Heterogeneity of Sedimentary Carbon in Mid-Latitude Fjords. *Front. in Earth Sci.* **7**, 269

43. Popp, B.N., Takigiku, R., Hayes, J.M., Louda, J.W., and Baker, E.W. The post-paleozoic chronology and mechanism of ^{13}C depletion in primary marine organic matter. *Am. Journal of Sci.* **289**, 436-454 (1989).

44. Meyers, P.A. Preservation of elemental and isotopic source identification of sedimentary organic matter. *Chem. Geol.* **114**, 289-302 (1994).

45. Lafargue, E., Marquis, F., Pillot, D. Rock-Eval 6 Applications in Hydrocarbon Exploration, Production, and Soil Contamination Studies. *Rev. l'Institut Fr. du Pet*. **53**, 421–437 (1998)

46. Cornford, C. Source rocks and hydrocarbons of the North Sea (11). In: Petroleum geology of the North Sea: Basic concepts and recent advances, 4th Edition. Edited by Glennie, K.W. *Blackwell Science* (1998).

47. Maende A. Wildcat compositional analysis for conventional and unconventional reservoir assessments HAWK petroleum assessment method (H-PAM)™. Application note (052016–1). (2016).

48. Bourbonniere, R.A. and Meyers, P.A. Sedimentaty geolopid records of historical changes in the watersheds and productivities of Lake Ontario and Erie. *Limnol. Oceanogr.* **41** (2), 352-359 (1996).

49. Taylor, G.H., Teichmüller, M., Davis, A., Diessel, C.F.K., Littke, R., Robert, P. Organic Petrology. Gebr. Borntraeger, Berlin-Stuttgart (1998).

50. Hartkopf-Fröder, C., Königshof, P., Littke, R., Schwarzbauer, J. Optical thermal maturity parameters and organic geochemical alteration at low grade diagenesis to anchimetamorphism: A review, *Int. J. of Coal Geol.* **150-151**, 74-119 (2015).

51. Pickel, W., Kus, J., Flores, D., Kalaitzidis, S., Christanis, K., Cardott, B., Misz-Kennan, J. Rodrigues, M., Hentschel, A., Hamor-Vido, M., Crosdale, P. Wagner, N. Classification of liptinite – ICCP System 1994, *Int. J. of Coal Geol.* **169**, 40-51 (2017).

52. Walther, J., 1894, Einleitung in die Geologie als historische Wissenschaft. In Lithogenesis der Gegernwart. *Jena: G. Fischer, Bd. 3, pp. 535-1055.*

53. Galy, V.V., Beyssac, O., France-Lanord, C., Eglington, T. Recycling of graphite during Himalyan erosion: a geological stabilization of carbon in the crust. *Science* **322**, 943-945 (2008).

54. Milliman, J.D., Syvitski, J.P.M. Geomorphic/tectonic control of sediment discharge to the ocean: the importance of small mountainous rivers. *The Journal of Geology* **100**, 525-544 (1992).

Methods

Field work and sampling

Fieldwork was conducted in February and March 2020 in Cerro Cazador, southern Patagonia, Chile (Extended Data Fig. 1). Two main sets of data were collected. First a series of aerial pictures were acquired using an uncrewed aerial vehicle (UAV) to build a digital outcrop model of the study area (see section 2; ref. 55). Second, a 525 m thick geologic section was measured and sampled to be analysed for organic geochemistry (sections 3 to 6).

The section was dug using shovels and a pickaxe to expose all beds and remove the vegetation cover. The section was divided into 5 sub-sections that were connected using continuously exposed beds (Extended Data Fig. 1). DGPS points were collected every 5 m along each sub-section and all points were imported into Google Earth (Extended Data Fig. 1c). Each sub-section was measured for sediment facies (e.g. grain size, presence of sedimentary structures) at a 10 cm resolution. The abundance of remains of organic matter visible to the naked eye was also recorded, yet these observations are only qualitative indications of the macroscopic debris and were thus not further used in our analysis.

Samples were systematically taken at 5 m intervals, and some additional samples were collected in facies of interest. In total, we collected 99 samples along the 525 m section. Samples were collected from rock outcrops by hammering. We removed an additional 20-30 cm of surface material from the trench at every sample location in order to access fresh surfaces, i.e. devoid of vegetation and modern soil. We took about 500 g of material for each sample. Extra care was taken for samples aimed to be analysed for biomarkers (section 6), *i.e.,* we used nitrile gloves and wrapped samples in aluminium foil to prevent contamination from any modern biomarkers. All samples were shipped to the Department of Geoscience, University of Calgary (Canada).Samples were washed and cut into 1 cm^3 cubes using a water-cooled rock saw. Once cleaned and cut, samples were ground into powder using an automated ball-mill grinder. Samples were

loaded into pots with agate balls and milled for 8 min at 250 rpm. After each run the agate balls were removed, and the powders were transferred into glass vials using a metal spatula. Pots and agate ball were cleaned with methanol and dried between runs.

Creation of a digital outcrop model to derive clinothem dimensions

An uncrewed aerial vehicle (UAV) was used to acquire images of the outcrops of interest at central Cerro Cazador (Extended Data Fig. 2) using a DJI Phantom 3 Professional quadcopter. More than 19,500 images were obtained by the UAV with primary camera angle parallel to the terrain and additional images captured from above and at angles oblique to the slope. Images were divided into subsets of 1,000-3,000 photos and used to generate a digital outcrop model (DOM) with a typical resolution of 0.03 – 0.04 m per pixel using Pix4D photogrammetric software. A series of natural points on the outcrop were recorded in the field using a differential global positioning system (dGPS). Surveyed points were used as ground control points (GCPs) within photogrammetric processing in order to constrain the scale, orientation, and location of the DOM[31, 55] . Stratigraphic surfaces were digitized, or traced, on the 3D point cloud within Pix4D and exported as shapefiles including location (x,y,z) attributes into ArcGIS software. Each line was projected onto a 2D plane oriented perpendicular to bedding in order to account for post-depositional tectonic effect on bedding geometry[31,56]. The projected lines resulted in a structurally restored 2D stratigraphic cross-section through the succession, oriented parallel to the depositional dip of the outcrop (*i.e.,* roughly north to south in central Cerro Cazador, Extended Data Fig. 2c). These stratigraphic surfaces were interpreted based on their continuity and on their composition in the measured section.

Three clinothems were identified, with their respective bottomset, foreset, and topset segments. The dip cross sectional area of each clinothem and each segment was measured in the outcrop model (Extended Data Fig. 2c). The measured section crosses the bottomset of clinothem 1, the foreset of clinothem 2, and the topset of clinothem 3 (Extended Data Fig. 2c). Topset, foreset, and bottomset

deposits from these three clinothems were thus considered collectively to form a composite clinothem record, from which a comprehensive OC burial budget was estimated using geochemical measurements described below.

Carbon stable isotopes data collection

Samples were measured for organic carbon stable isotopes ($\delta^{13}C$) composition and total organic carbon content (TOC) using an elemental analyser – isotope ratio mass spectrometer (EA-IRMS) at the University of Calgary (Fig. 3). Prior to these measurements, carbonates were removed from the samples because combustion within the EA-IRMS decomposes carbonate minerals into inorganic CO_2, which affects the isotopic composition measured on the organic matter[57]. We leached all samples with 10% hydrochloric (HCl) acid and let the reaction last for 2 hours. Fifteen of the 99 samples reacted with HCl. Leached samples were washed with deionised water and centrifuged three times to remove any trace of HCl. Samples were then transferred back into glass vials and dried in an oven at 55 °C for 72 hrs. Dried decarbonated samples were scraped from the vials and homogenised using a glass spatula. Between 6 and 8 mg were weighed for each sample and placed into tin capsules prior to being inserted into the EA-IRMS and measured for TOC and $\delta^{13}C$.

Carbon stable isotopes are commonly used to identify the presence of terrestrial plants and marine organic matter in marine sediments[58,59] . Plants produce organic matter via consumption of atmospheric CO_2 through photosynthesis whereas marine phytoplankton use oceanic inorganic carbon, introducing an isotopic fractionation difference between organic matter types[43,44]. Common C3 land plants lead to the production of terrestrial organic matter with $\delta^{13}C$ values of about -30 to -24‰ whereas marine organic matter has values between -24 and -18‰[43,44,59]. Mixture of terrestrial and marine organic matter in oceanic sediments thus leads to average $\delta^{13}C$ values that overlaps between sources; it is therefore

important to use other indicators to separate terrestrial from marine organic matter (e.g. HAWK-derived indices[43]).

HAWK pyrolysis data collection

Programmed pyrolysis analysis was performed on all samples at the Geological Survey of Canada (Calgary) using the standard cycle of a Wildcat Technologies HAWK Pyrolysis and TOC Instrument (Fig. 3, Extended Data Fig. 4). Approximately 80 mg of whole rock sample was powdered and heated first to a temperature of 300 °C under an inert atmosphere for 3 minutes followed by increasing temperature at a rate of 25 °C per minute to a final temperature of 650 °C. This initial pyrolysis stage measured the amount of free hydrocarbons (S1 peak), residual hydrocarbon potential/kerogen content (S2 peak), and hydrocarbons containing oxygen (S3 peak) present in each sample. Hydrogen (HI) and Oxygen (OI) indices were derived from S2 and S3 peaks to provide an indication of relative hydrogen and oxygen content and interpreted for the organic matter origin and maturity[46,60] (Extended Data Fig. 4c,d). Typically, low hydrogen indices and high oxygen indices are interpreted as predominantly terrestrial organic matter[43]. The sample was then exposed to oxygen and heated from 300 °C to 850 °C in the oxidation stage. The residual carbon from this stage and pyrolyzable carbon were added to determine the TOC content of the sample[45,47,61,62]. Although programmed pyrolysis methods have been widely used for oil and gas exploration (Extended Data Fig. 5), they are now increasingly being used for characterisation of organic matter in the deep-sea[38].

Organic petrography and vitrinite reflectance

12 samples were prepared into polished pellets using a cold-setting epoxy resin at the Geological Survey of Canada (Calgary) for organic petrographic analysis. Samples were examined using a Zeiss Axioimager II Microscope system equipped with white and ultra-violet light sources and the Hilgers Technisches Büro Diskus-Fossil system. Measurements of reflectance were made on macerals across the surface of all 12 sample pellets in white light using a 0.86 μm^2 measurement spot size under oil immersion (Immersol 518,

ne = 1.518 at 23 °C), using a 50x objective, calibrated to yttrium-aluminum-garnet with a standard R_o of 0.906%. Reflectance measurements were randomized and measured at a light wavelength of 546 nm following the procedure outlined in ASTM D7708-14 (ASTM, 2014). Vitrinite Reflectance (VR_o) of the measured samples range between 0.48 ± 0.05 % to 0.72 ± 0.1 %VR_o (Extended Data Fig. 6c), indicating a thermal maturity ranging from immature to the early catagenetic stage[46].

Biomarkers

Twelve samples were analyzed for biomarkers at the Petroleum Reservoir Group (PRG), Department of Geoscience, University of Calgary (see Figs 2 and S3 for sample locations). 50 g of each sample were ground and Soxhlet extracted for 72 hrs with dichloromethane (DCM). The extract was separated into aliphatic hydrocarbon and aromatic hydrocarbon fractions using solid phase extraction techniques. Each aliphatic fraction was analysed using an Agilent Gas Chromatograph Mass Spectrometer (7890B GC + 5977 MS). The GC oven was programmed to heat from 30 °C to 325 °C at 4 ° min^{-1}. The MS was operating in a simultaneous selected ion monitoring (SIM) SCAN mode, scanning from 50–550 mz and collecting 60 selected ions. Using the SIM data, peaks of interests were identified and integrated using the Agilent Chemstation software.

n-alkanes identified in the extracted hydrocarbons inform the sources of the organic matter, e.g. long-chain alkanes C_{27}, C_{29} and C_{31} indicate the presence of land-plant epicuticular waxes[63] whereas short-chain C_{15}, C_{17} and C_{19} show the presence of algal contributions[64]. The ratio between long-chain and short-chain alkanes was thus used to derive the terrigneous to aquatic ratio as follows (TAR[48]; Extended Data Fig. 5b):

$$TAR = (C_{27} + C_{29} + C_{31}) / (C_{15} + C_{17} + C_{19})$$

Higher TAR values thus indicate land-derived organic matter[48].

Calculation of organic carbon mass, annual fluxes and annual yields

The steps we used to calculate OC mass, fluxes and yields are detailed in Extended Data Table 2 for each of the clinothem segment and for the composite clinothem.

In order to estimate the mass of OC buried in the composite clinothem (M_{oc}), we need to calculate (Extended Data Table 2a):

$$\mathbf{M_{OC} = TOC * D * W * (1-\varphi) * \rho} \qquad \mathbf{(1)}$$

Where D is 0.47 km^2 and corresponds to the dip cross sectional area, measured based on the DOM. W is the estimated width of the clinothem in km. This dimension being difficult to constrain, we use a minimum estimate of 6 km corresponding to two times the clinothem length based on ref. 30 and a maximum estimate of 20 km corresponding to the approximate basin width[26], averaging 13 ± 7 km. TOC is the total organic carbon content in % calculated from the average TOC of samples collected in the interpreted bottomsets, foresets and topsets of the clinothem. φ is the porosity and varies between 5 and 20% for the mud-dominated deposits (bottomsets) and sand-dominated deposits (foresets and topsets), respectively[35]. ρ is the sediment density in kg m^{-3}. The deposits being dominated by silicates, we use the density of the quartz (2650 kg m^{-3}).

In order to estimate how much OC is buried annually in the clinothem, we use (Extended Data Table 2b):

$$\mathbf{OC\ annual\ flux = TOC * A * SR * (1-\varphi) * \rho} \qquad \mathbf{(2)}$$

Where A corresponds to the surface area (i.e., in plan-view) of the clinothem. Given the little constraints on the clinothem width, we derived 2 surface area scenarios ranging between 8.5 and 23.8 km^2. TOC, φ and ρ are the same parameters as in equation (1).

SR is the vertical sedimentation rate in m/yr. The SRs used are based on a compilation of SRs reported from the literature in subaqueous clinothems reported from both ancient successions (encompassing Myr timescales) and modern river-connected clinothems (formed and active in the Holocene; Extended

Data Table 1). SRs reported in Holocene settings are typically an order of magnitude faster (0.1 to 10 cm yr^{-1}; Extended Data Table 1) compared to the ancient successions (0.07 to 1 mm yr^{-1}: Extended Data Table 1). We explained this difference by the methods used to date Holocene and ancient deposits which cover different durations (maximum a century for Holocene settings and millions of years for ancient settings, Extended Data Table 1). Further, this trend of decreasing SR with increasing time span was previously highlighted globally for linear sedimentation rates in various depositional environments[65]. In order to be conservative and inclusive of all study cases considered in Extended Data Table 1, we used a minimum SR of 0.15 mm yr^{-1} (i.e., slow scenario) based on the mean SR reported in ancient successions, and a maximum SR of 1 mm yr^{-1} (i.e., fast scenario) based on the minimum SR reported in Holocene settings. A few study cases presented different SRs between topset, foreset, and bottomset segments. However, we chose to use a mean SR for the entire clinothem for simplicity. Using the average thickness of the composite clinothem (130 m), the fast SR scenario results in a duration of 0.1 Myr while the slow SR scenario results in a duration of 0.9 Myr for our studied clinothem. This duration range is consistent with 1) detrital zircon geochronology (U-Pb dating) performed a few hundred meters below and above our study section which resulted in a duration of 0.5 ± 1.7 Myr[33], and 2) the expected 10^4 to 10^6 durations for shelf-edge delta scale clinothems[14].

Data availability: All data needed to evaluate the conclusions in the paper are present in the data source associated with the paper. Data and metadata associated with organic carbon measurements made on the marine sediment samples can also be found at PANGAEA REPOSITORY DOI (waiting for a DOI, data submitted on 16/08/22).

Methods-only references

55. Nesbit, P.R., Durkin, P.R., Hugenholtz, C.H., Hubbard, S.M., Kucharczyk, M. 3-D stratigraphic mapping using a digital outcrop model derived from UAV images and structure-from-motion photogrammetry. *Geosphere* **14** (6), 2469–2486 (2018).

56. Englert, R.G., Hubbard, S.M., Coutts, D.S. & Matthews, W.A. Tectonically controlled initiation of contemporaneous deep-water channel systems along a Late Cretaceous continental margin, western British Columbia, Canada. *Sedimentology,* **65(7),** 2404–2438 (2018).
57. Hilton, R.G., Galy, A., Hovius, N., Horng M-J., Chen, H. The isotopic composition of particulate organic carbon in mountain rivers of Taiwan. *Geochem. & cosm. Acta* **74**, 3164-3181 (2010).
58. Spiker, E.C. Carbon isotopes as indicators of the source and fate of organic carbon in rivers and estuaries. In: Flux of organic carbon by rivers to the oceans. *Report of a Workshop, Woods Hole, MA,* Sept 21-25, 75-108 (1981).
59. Gaines, S.M., Eglinton, G., and Rullkotter, J., Echoes of Life: What Fossil Molecules Reveal about Earth History: *Oxford, UK, Oxford University Press*, 355 p. (2009)
60. Jarvie, D. Correlation of Tmax and measured vitrinite reflectance. *TCU Energy Institute* (2018).
61. Espitalié, J., Laporte, J.L., Madec, M., Marquis, F., Leplat, P, and Paulet, J. Méthode rapide de caractérisation des roches mères, de leur potentiel pétrolier et de leur degré d'évolution. *Rev. Inst. Fr. petr.* **32**, 32-45 (1977).
62. Behar, F., Beaumont, V., and De B. Penteado, H.L. Rock-eval 6 Technology: performances and developments. *Oil & Gas Sci. & Techn. – Rev. IFP* **56** (2), 111-134 (2001).
63. Eglington, G. and Hamilton, R.J Leaf epicuticular waxes. *Science* **156**, 1322-1335 (1967).
64. Blumer, M.R. Guillard, R.L., Chase, T. Hydrocarbons of marine plankton. *Mar. Biol.* **8**, 183-189 (1971).
65. Sadler, P. M. (1981). Sediment Accumulation Rates and the Completeness of Stratigraphic Sections. *The Journal of Geology*, **89**(5), 569–584. doi:10.1086/628623
66. Browning, J.V., Miller, K.G., Sugarman, P.J., Barron, J., McCarthy, F.M.G., Kulhanek, D.K., Katz, M.E., Feigenson, M.D. (2013) Chronology of Eocene–Miocene sequences on the New Jersey shallow shelf:

Implications for regional, interregional, and global correlations. *Geosphere* **9** (6): 1434–1456. doi: https://doi.org/10.1130/GES00857.1

67. Cosgrove, G.I.E., Hodgson, D.M., Poyatos-Moré, M., Mountney, N.P., McCaffrey, W.D.; Filter Or Conveyor? Establishing Relationships Between Clinoform Rollover Trajectory, Sedimentary Process Regime, and Grain Character Within Intrashelf Clinothems, Offshore New Jersey, U.S.A.. *Journal of Sedimentary Research* 2018;; 88 (8): 917–941. doi: https://doi.org/10.2110/jsr.2018.44
68. Paulissen, W.E., Luthi, S.M., Grunert, P, Coric, S., Harzhauser, M. (2011). Integrated high-resolution stratigraphy of a middle to late Miocene sedimentary sequence in the central part of the Vienna Basin. *Geologica Carpathica* **62** (2), 155-169. doi: 10.2478/v10096-011-0013-z
69. Borzi, A., Harzhauser, M., Piller, W.E., Strauss, P., Siedl, W., Dellmour, R. (2022). Late Miocene evolution of the Paleo Danube Delta (Vienna basin, Austria). *Global and Planetary Change* **210** https://doi.org/10.1016/j.gloplacha.2022.103769
70. Lease, R.O., Houseknecht, D.W., Kylander-Clark, A.R.C. (2022) Quantifying large-scale continental shelf margin growth and dynamics across middle-Cretaceous Arctic Alaska with detrital zircon U-Pb dating. *Geology* https://doi.org/10.1130/G49118.1
71. Thompson, R. and Cameron, T.D.J. (1995). Palaeomagnetic study of Cenozoic sediments in North Sea boreholes: an example of a magnetostratigraphic conundrum in a hydrocarbon producing area. *Palaeomagnetic Applications in Hydrocarbon Exploration and Production, Geological Society Special Publications* **98**, 223-236.
72. Neill, C.F., and Allison, M.A. (2005). Subaqueous deltaic formation on the Atchafalaya Shelf, Louisiana. *Marine Geology* **214**, 411-430. doi:10.1016/j.margeo.2004.11.002
73. Hart, B.S., Hamilton, T.S., Barrie, J.B. (1998). Sedimentation rates and patterns on a deep-water delta (Fraser Delta, Canada): integration of high-resolution seismic stratigraphy, core lithofacies, and ^{137}Cs fallout stratigraphy. *Journal of sedimentary Research* **68** (4), 556-568.

74. Bassetti, M.A., Berné, S., Jouet, G., Taviani, M., Dennielou, B., Flores, J.-A., Gaillot, A., Gelfort, R., Lafuerza, S., Sultan, N. (2008). The 100-ka and rapid sea level changes recorded by prograding shelf sand bodies in the Gulf of Lions (wester Mediterranean Sea). *Geochemistry, Geophysics, Geosystems* **9**(11), 27p.

75. Berné, S., Jouet, G., Bassetti, M.A., Dennielou, B., Taviani, M. (2007). Late Glacial to Preboreal sea-level recorded by the Rhone deltaic system (NW Mediterranean). *Marine Geology* **245**, 65-88.